Local and Distributed Voltage Control Algorithms in Distribution Networks

Guido Cavraro and Ruggero Carli, *Member, IEEE*

***Abstract*—In this paper, we consider a voltage control problem in power distribution grids. The specific goal is that of keeping the voltages within preassigned operating limits by commanding the reactive power output of the microgenerators connected to the grid. We propose three strategies. The first two strategies are purely local, meaning that each microgenerator updates the amount of reactive power to be injected based only on local measurements of the voltages' magnitude. Instead the third one is distributed, namely, the microgenerators, to perform the updating steps, require some additional information coming from the neighboring agents. The local strategies are simpler to be implemented, but they might fail in solving the voltage control problem. Instead, the distributed one requires the microgenerators to be endowed with communication capabilities, but it is effective in driving the voltages within the admissible intervals and, additionally, it exploits the cooperation among the agents to reach also a power losses minimization objective. Theoretical analysis and extensive numerical simulations are provided to confirm the arguments aforementioned.**

***Index Terms*—Power distribution systems, reactive power control, voltage control, Volt/VAR control.**

I. Introduction

RECENT technological advances, together with environmental and economic challenges, have been motivating the massive deployment of small power generators in the low voltage and medium voltage power distribution grid [1]. On one hand, significant benefits to the network operation could come from the availability of a large number of these generators in the distribution grid; indeed, they might provide a number of ancillary services, e.g., voltage profile improvements, reduction of line losses, reduction of power generation cost, just to mention a few [2], that are of great interest for the grid management. On the other hand, the uncontrolled injection of power from several renewable energy sources can cause serious system damages or system instabilities. For instance, operational bounds may be violated due to the intermittence of the renewable sources, as large voltages variations might occur. For these reasons, voltage regulation is a fundamental issue in the development of the future *smart distribution grid*.

Traditionally, in power transmission systems voltage regulation is achieved through a hierarchical control architecture; precisely, a layering of primary, secondary, and tertiary control [3], [4]. The goal of primary control is that of balancing generation and demand, synchronizing the AC voltage frequencies, and stabilizing their magnitudes. This is accomplished via decentralized droop control, where generators are controlled such that their power injections are proportional to their voltage frequencies and magnitudes. Droop controllers induce steady-state errors in frequency and voltage magnitudes, which are corrected in a secondary control layer. The transmission network is divided into control areas in which a bus is elected to be the pilot bus. Secondary voltage control strategies aim at supporting the pilot bus voltage through PI controllers that generate the reactive power output of each generator within the area through a feedback on the corresponding pilot voltage. The operating point stabilized by primary/secondary control is scheduled in a tertiary control layer, to establish fair load sharing among the sources, or to optimize voltage profiles at the bus, minimizing suitable functional costs, e.g., power losses. Usually, optimal configuration is computed offline by a central unit (TSO), using precise load forecasts. However, techniques that update such optimal configuration, based on field measurements in a closed loop real time control system, have been developed [3]. Primary, secondary, tertiary controls work on different timescales: seconds for the primary, few minutes for the secondary, some minutes for the tertiary. While the hierarchical architecture has been adapted from the transmission level to microgrids, the control challenges and architecture limitations imposed by the microgrid framework are as diverse as they are daunting. The low levels of inertia means that primary control must be fast and reliable to maintain voltages, frequencies, and power flows within acceptable tolerances, while microgrid controllers must be able to adapt in real time to unknown and variable loads and network conditions. In short, the three layers of the control hierarchy for microgrids should allow for as close to plug-and-play operation as possible, be either distributed or completely decentralized, and operate seamlessly without a separation of time scales [5].

In the past, electro-mechanical control devices, such as shunt capacitor banks or on-load tap changers [6], have been used to perform voltage control in distribution grids. However, they are typically too slow to properly respond to voltage fluctuations due to the loads or energy resources high variability, while inverters can act on a fast timescale. This has motivated the recent increasing interest for strategies that regulate the voltage magnitudes by directly actuating the injection (or absorption) of the microgenerators reactive power; indeed, when running below their

Manuscript received August 30, 2016; revised January 20, 2017 and May 24, 2017; accepted July 8, 2017. Date of publication July 26, 2017; date of current version February 16, 2018. Paper no. TPWRS-01312-2016. *(Corresponding author: Guido Cavraro.)*

G. Cavraro is with the Department of Electrical and Computer Engineering, Virginia Tech, Blacksburg, VA 24061 USA (e-mail: cavraro@vt.edu).

R. Carli is with the Department of Information Engineering, University of Padova, Padova 35122, Italy (e-mail: carlirug@dei.unipd.it).

Digital Object Identifier 10.1109/TPWRS.2017.2731682

rated output current, many inverters can inject (or of absorb) reactive power together with active power [7]. Recently, there has been a growing literature proposing strategies for rapidly regulating the injections of the micro-generators reactive power to deal with the voltage regulation problem. These strategies are both *purely local* and *distributed*. *Purely local* means that agents use just local measurements and do not exchange information with each other; *distributed* means that agents, that are physically close, are allowed to communicate and can share information to cooperatively reach the pre-assigned objectives. Purely local strategies (see [8]–[14]) mainly aim to guarantee that voltage constraints are satisfied. Distributed strategies (see [15]–[18]), beside local voltage constraints, take into account other important global objectives, e.g., power losses minimization, and drive the state system towards configurations which are obtained solving the so-called *optimal reactive power flow* (ORPF) problems. Strategies in [15]–[17] reformulate ORPF problems as a rank-constrained semidefinite programs, convexify them and provide solutions in a distributed manner through standard optimization algorithms. However, these approaches require the monitoring of all the buses of the grid, which, in general, is not amenable of practical implementation in the distribution grid. This issue is overcome in [18] where not all the buses are required to be monitored. The algorithm proposed in [18] is based on the alternating actuation of the two following steps: gathering voltage measurements at the micro-generators buses and applying control laws based on these measured data.

Three voltage control strategies are proposed in this paper. Two strategies (denoted as LVC-1 and LVC-2) are purely local. They exhibit a fast transient properties and are shown to converge to a steady state which, in general, is not guaranteed to meet the voltage constraints. At this regard, we provide a numerical example where, for both LVC-1 and LVC-2, the micro-generators fail in regulating the voltage within the desired limits, even if a proper reactive power dispatch would allow it. This issue is overcome by the third strategy (denoted as f-DORPF) which is a novel distributed algorithm improving the performance of the distributed strategy introduced in [18] (denoted as DORPF). Remarkably, in [18], it is shown that adding information exchanges between neighboring nodes allows the DORPF algorithm to solve the voltage control problem while also reaching a power losses minimization objective. However DORPF exhibits poor transient performance, namely, it requires a consistent number of iterations to approach the optimal solution. The main idea behind the f-DORPF is that of combining the updating steps of DORPF with those of the purely local strategy LVC-2, thus obtaining fast transient properties, the operating conditions meeting and the power losses minimization.

The paper is organized as follows. A model of the distribution network is provided in Section III. In Section IV, we introduce the problem of regulating the voltages magnitudes through the reactive power injected by the micro-generators. In Section V and in Section VI, we illustrate, the proposed strategies. Finally, we analyze and compare the performance of the various strategies in Section VII.

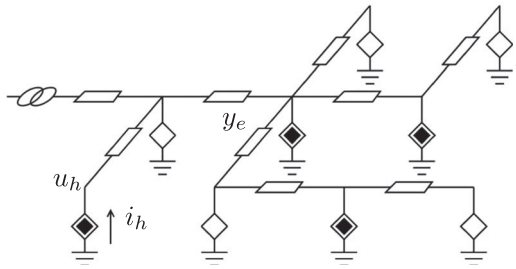

Fig. 1. Circuital representation of a microgrid, where black diamonds are micro-generators, white diamonds are loads, and the left-most element of the circuit represents the PCC.

II. Notation and Mathematical Preliminaries

Let us denote by $\mathcal{G} = (\mathcal{V}, \mathcal{E})$ a undirected graph, where $\mathcal{V}$ and $\mathcal{E}$ represent the set of nodes and the set of edges, with $n = |\mathcal{V}|$ and $r = |\mathcal{E}|$. Given two nodes $h, k \in \mathcal{V}$, we define the path $\mathcal{P}_{hk} = (v_1, \dots, v_\ell)$, with $v_1 = h$, $v_\ell = k$, as the sequence of nodes, without repetitions, such that v_i and v_{i+1} are connected by an edge, for each $i = 1, \dots, \ell - 1$. Given a vector u, $\bar{u}$ denotes its complex conjugate, while u^T denotes its transpose. Instead, $\Re(u)$ and $\Im(u)$ refer to its real and imaginary part (element-wise), respectively. Let the symbol $\mathbf{1}$ denote the column vector whose elements are all equal to one, while the symbol e_v denote the column vector whose elements are all equal to 0, except its v-th entry which is equal to 1. Given $w, \underline{w}, \overline{w} \in \mathbb{R}^\ell$, with $\underline{w}_h \leq \overline{w}_h, h = 1, \dots, \ell$, let the operator $[w]_{\underline{w}}^{\overline{w}}$ be the component-wise projection of u in the set $\left\{x \in \mathbb{R}^\ell : \underline{w}_h \leq x_h \leq \overline{w}_h, h = 1, \dots, \ell\right\}$, that is,

$$([w]_{\underline{w}}^{\overline{w}})_h = \begin{cases} w_h \text{ if } \underline{w}_h \leq w_h \leq \overline{w}_h \\ \underline{w}_h \text{ if } w_h < \underline{w}_h \\ \overline{w}_h \text{ if } w_h > \overline{w}_h. \end{cases} \tag{1}$$

Given a real number x we define the function $\text{sign}(x)$ as

$$\text{sign}(x) = \begin{cases} x/|x| \text{ if } x \neq 0 \\ 0 \quad \text{if } x = 0. \end{cases} \tag{2}$$

Given a matrix Λ, we denote with $\rho(\Lambda)$ its spectral radius, namely, the largest eigenvalue in absolute value.

III. Smart Grid Cyber-Physical Model

In this paper, we describe the *smart* power distribution network as a cyber-physical system, where the *physical layer* is composed by the power distribution infrastructure including the electric lines, micro-generators, loads and the point of connection to the transmission grid (denoted as PCC), while the *cyber layer* consists of the intelligent agents which are deployed in the electric grid.

A convenient way to model the physical layer is by a directed graph $\mathcal{G}$, where edges in $\mathcal{E}$ represent the electric lines, and nodes in $\mathcal{V}$ represent both loads and generators connected to the microgrid (see Fig. 1). The following variables describe the overall state of the system:

1) $u \in \mathbb{C}^n$, where u_h is the voltage at node h;
2) $v \in \mathbb{R}^n_{\geq 0}$, where v_h is the voltage magnitude at node h;

3) $i \in \mathbb{C}^n$, where i_h is the current that node h injects;
4) $s = p + jq \in \mathbb{C}^n$, where s_h, p_h and q_h are the complex, the active and the reactive power injected at node h.

We model the PCC as an ideal sinusoidal voltage generator (*slack bus*) at the grid nominal voltage U_N. Without loss of generality, we label the PCC as node 1 and we assume its voltage phase to be equal to 0. The powers s_h corresponding to grid loads are such that $p_h < 0$, which means that active power is *supplied* to the devices, while, when dealing with power micro-generators, we have that $p_h \geq 0$, which means that active power is *injected* into the grid. The system state satisfies the following relations

$$i = Yu, \qquad u_1 = U_N, \tag{3}$$

$$u_h \bar{i}_h = p_h + jq_h \qquad h \neq PCC, \tag{4}$$

where Y is the bus admittance matrix of the grid. The element Y_{hk} represents the admittance of the line connecting bus h with bus k. The Green matrix $X \in \mathbb{R}^{n \times n}$, depending only on the topology of the grid power lines and on their impedances, is the unique symmetric positive semidefinite matrix ([18]) s.t.

$$u = Xi + \mathbf{1}U_N. \tag{5}$$

In our setup, each micro-generator corresponds to an *agent* in the cyber layer and belongs to the set $\mathcal{C} \subseteq \mathcal{V}$ (with $|\mathcal{C}| = m$). We assume that the agents are provided with *sensing capabilities*, in particular *voltage phasor measurement units* (PMU) (devices that measure both magnitude and phase of the voltages) and with *computational capabilities* that will be exploited in the proposed algorithms implementation. In particular, the agents can regulate the amount of reactive power injected into the grid. To underline the difference among smart agents and passive loads, we adopt the following block decomposition of the voltage vector u

$$u = \left[u_1 \; u_G^T \; u_L^T \right], \tag{6}$$

where u_1 is the voltage at the PCC, $u_G \in \mathbb{C}^m$ are the voltages at the micro-generators, and $u_L \in \mathbb{C}^{n-m-1}$ are the voltages at the loads. Similarly, $s_G = p_G + jq_G$ and $s_L = p_L + jq_L$. Following the same partitioning, we can block-partition X as

$$X = \begin{bmatrix} 0 & 0 & 0 \\ 0 & M & N \\ 0 & N^T & Q \end{bmatrix},$$

where $M \in \mathbb{C}^{m \times m}, N \in \mathbb{C}^{m \times n-m-1}, Q \in \mathbb{C}^{n-m-1 \times n-m-1}$. The non-linear relation between u and s, can be conveniently linearized as in [18], by

$$\begin{bmatrix} u_G \\ u_L \end{bmatrix} = \frac{1}{U_N} \begin{bmatrix} M & N \\ N^T & Q \end{bmatrix} \begin{bmatrix} \bar{s}_G \\ \bar{s}_L \end{bmatrix} + \mathbf{1}U_N. \tag{7}$$

Interestingly, (7) can be used to approximate the voltages magnitudes as

$$\begin{bmatrix} v_G \\ v_L \end{bmatrix} = \frac{1}{U_N} \Re \begin{bmatrix} M & N \\ N^T & Q \end{bmatrix} \begin{bmatrix} p_G \\ p_L \end{bmatrix} + \frac{1}{U_N} \Im \begin{bmatrix} M & N \\ N^T & Q \end{bmatrix} \begin{bmatrix} q_G \\ q_L \end{bmatrix} + \mathbf{1}U_N. \tag{8}$$

Equation (8) represents a more general version of the widely used *linearized DistFlow model* (e.g., in [10], [11], [13]), which holds also in the case of no radial grids. Equations (7) and (8) will be used in the following to model the grid voltages and their magnitude, respectively.

IV. Voltage Control Strategies Based on Reactive Power Regulation

Classically, the generators regulate the amount of reactive power they inject into the electrical grid, in order to perform the *voltage control*, i.e., to maintain the voltage magnitudes of the buses within a predefined deviation from the nominal voltage U_N. Since we assume that only agents can take voltage measurements, we aim at meeting the following constraints

$$U_{\min} \leq v_h \leq U_{\max}, \qquad \forall\, h \in \mathcal{C}. \tag{9}$$

where $U_{\min}$ and $U_{\max}$ denote, respectively, the minimum and maximum admissible values for the voltages magnitude. Usually, $U_{\min} = (1-\xi)U_N$ and $U_{\max} = (1+\xi)U_N$, where $0 < \xi < 1$. In addition, since typically the generators dispersed in the distribution network are of small size, we take into account also constraints on the generation capability of agent h. Specifically, we assume

$$q_{\min,h} \leq q_h \leq q_{\max,h}, \qquad \forall\, h \in \mathcal{C}, \tag{10}$$

where $q_{\min,h}$, $q_{\max,h}$ are, respectively, the minimum and the maximum amount of reactive power that agent h can inject. Typically $q_{\min,h} < 0$, $q_{\max,h} > 0$ and $q_{\min,h} = -q_{\max,h}$. For the sake of simplicity and in order to keep the notation lighter, in the following, we will assume that the micro-generators are homogeneous, namely, for all $h \in \mathcal{C}$,

$$q_{\min,h} = q_{\min}, \qquad q_{\max,h} = q_{\max},$$

for given $q_{\min}, q_{\max}$. Based on the constraints in (9) and in (10), we introduce a proper definition of the set of the *feasible reactive power injections*. Observe that, in the setup we described, the quantities p_G, p_L and q_L are assumed to be constant and that only q_G is actuated in order to regulate v_G. Hence, for a given triple (p_G, p_L, q_L), we define

$$\mathcal{F}(p_G, p_L, q_L) = \{q_G \text{ such that for all } h \in \mathcal{C} \text{ it holds } q_{\min} \leq q_h \leq q_{\max}, U_{\min} \leq v_h \leq U_{\max}\}.$$

Since there is no risk of confusion, for the sake of notational convenience, we omit the dependence of $\mathcal{F}$ on (p_G, p_L, q_L).

In next sections we introduce three strategies, where each agent updates the amount of reactive power to be injected in order to maintain the voltages magnitudes within the interval $[U_{\min}, U_{\max}]$. The first two strategies are *purely local*, i.e.,

1) agent h updates q_h based only on measurements of the magnitude of its own voltage, that is, v_h;
2) there is no exchange of information between the agents.

In the third strategy, instead, agents can communicate with each other ; the exchange of information regards the taken measurements and some additional quantities, as we will describe in Section VI. To properly model the admissible communications

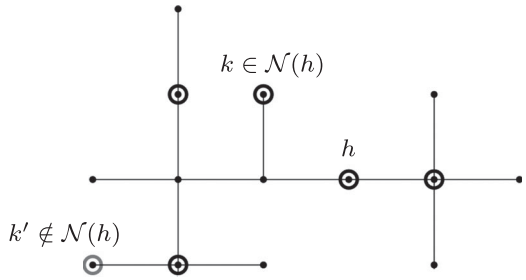

Fig. 2. An example of neighboring cyber layer agents. Circled nodes represent agents. The black circled nodes belong to $\mathcal{N}(h)$, while the gray circled node do not. For each agent $k \in \mathcal{N}(h)$, there exists a path that connects h to k which does not include any other agent.

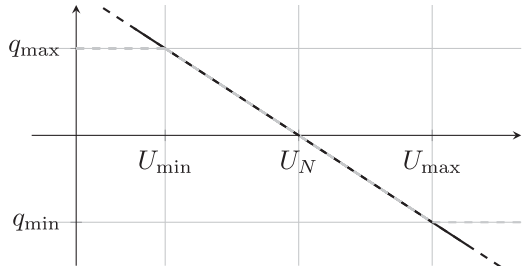

Fig. 3. Pictorial representation of f (black solid line) and $\hat{f}$ (gray dashed line), in the particular case where $q_{\max} = q_{\min}$ and $U_{\min} = (1-\xi)U_N$, $U_{\max} = (1+\xi)U_N$.

in the cyber layer, we next define the set of neighbors of a given agent h.

Definition 1: Let $h \in \mathcal{C}$ be an agent. The set of neighbors of h, denoted as $\mathcal{N}(h)$, is the subset of $\mathcal{C}$ defined as

$$\mathcal{N}(h) = \{k \in \mathcal{C} \cup \{1\} \mid \exists\, \mathcal{P}_{hk}, \mathcal{P}_{hk} \cap \mathcal{C} = \{h,k\}\}\,.$$

In Fig. 2 we report an example of the neighbors set. In our setup we assume that every agent $h \in \mathcal{C}$ knows its neighbors, i.e., $\mathcal{N}(h)$, and that it can communicate with them.

Remark 1: The communication among agents can be modeled by the *communication graph* $\mathcal{G}_C = \{\mathcal{C}, \mathcal{E}_C\}$, in which the vertexes are the smart agents, and in which every edge connects two neighbors agents able to communicate. It is possible to see that the graph $\mathcal{G}_C$ is the *kron reduction* [19] of $\mathcal{G}$ w.r.t. the set of smart nodes $\mathcal{C}$, and that it is a connected graph.

V. Purely Local Voltage Control Strategies

In this section we propose two control strategies where each agent h updates q_h exploiting only measurements of its own voltage magnitude, i.e., v_h.

A. A First Local Voltage Control Strategy (Denoted as LVC-1)

LVC-1 is a modified version of the reactive power compensation technique introduced in [7]. To formally describe LVC-1, let $f(v)$ be defined as

$$f(v) = \zeta v + \beta$$

and be such that

$$f(U_{\min}) = q_{\max},\ f(U_{\max}) = q_{\min}. \tag{11}$$

That is,

$$\zeta = -\frac{q_{\max} - q_{\min}}{U_{\max} - U_{\min}},\ \ \beta = \frac{q_{\max}U_{\max} - q_{\min}U_{\min}}{U_{\max} - U_{\min}}. \tag{12}$$

In addition, let $\hat{f}(v)$ be the saturated version of $f(v)$ outside the interval $[q_{\min}, q_{\max}]$, that is,

$$\hat{f}(v) = [f(v)]_{q_{\min}}^{q_{\max}}\,.$$

In Fig. 3, we provide a pictorial representation of f and $\hat{f}$. After having taken the measurement $v_h(t)$, $q_h(t)$ is updated by the h-th agent in the following way

$$q_h(t+1) = [q_h(t) + \alpha\,(\,f\,(v_h(t)) - q_h(t))]_{q_{\min}}^{q_{\max}} \tag{13}$$

where α is a positive constant. Observe that the equilibrium points for (13) are described by $\hat{f}(v)$; in fact, if $q_h(t) = \hat{f}(v_h(t))$ then $q_h(t+1) = q_h(t)$. In the particular case in which the minimum injectable reactive power is the opposite of the maximum, and the allowed voltage deviations are symmetric w.r.t. the nominal voltage value, i.e. $q_{\min} = -q_{\max}$, $U_{\min} = (1-\xi)U_N$ and $U_{\max} = (1+\xi)U_N$, then

$$\zeta = -q_{\max}/(\xi U_N), \qquad \beta = q_{\max}/\xi,$$

and it holds true that $\hat{f}(U_N) = 0$.

The following Proposition characterizes the convergence properties of (13).

Proposition 1: Consider algorithm (13) Then, if

$$\alpha \leq \frac{2}{1 - \frac{\zeta\rho(\Im(M))}{U_N}}, \tag{14}$$

there exists a m-upla $(\bar{v}_1, \ldots, \bar{v}_m)$ such that $v_h(t) \to \bar{v}_h$ and $q_h(t) \to \hat{f}\,(\bar{v}_h)$ for all $h \in \{1, \ldots, m\}$.

The proof of Proposition 1 is reported in the Appendix. In general, LVC-1 it does not guarantee that $\bar{v}_h$ lies within the interval $[U_{\min}, U_{\max}]$. If α satisfies condition (14), then each v_h converges to a steady-state $\bar{v}_h$ that, in general, might violate the constraints (9). In Section VII, we will provide a numerical example where, for some h, $\bar{v}_h \notin [U_{\min}, U_{\max}]$.

Remark 2: As previously said, LVC-1 is based on the strategy proposed in [7], which mimes the classical primary control schemes used in transmission networks, and complies also the IEEE 1547.8 standard [20]. In [7], q_h is updated as

$$q_h(t+1) = \hat{f}(v_h(t)), \tag{15}$$

i.e., q_h is set directly equal to the value dictated by the function $\hat{f}$. However, as remarked also by the authors of [7], the practical execution of (15) could lead to oscillatory and unstable behaviors. Moreover, as shown in [13], where the convergence of the algorithm proposed [7] has been analyzed, the slope of $f(v)$ must be small enough to ensure system stability. That is, it may happen that ζ must be much smaller than the value in (12) in such a way that (11) does not hold, (i.e., $f(U_{\min}) < q_{\max}$, $f(U_{\max}) > q_{\min}$), thus resulting in a partial utilization of the agents' generation capabilities, which is instead avoided by the *integral* rule (13).

Remark 3: Other purely local strategies have been proposed in the literature. The algorithm in [10] is provably shown to

drive the voltages into the operating intervals defined in (9); however the analysis in [10] is carried on only in the limited scenario where all the agents are assumed to be compensators and where no limits on the reactive powers are taken into account. Instead, the algorithms proposed in [12], [13] assume the constraints in (10) to hold for all the compensators; these algorithms, similarly to LVC-1 are theoretically proved to converge to a steady-state which, however, is not guaranteed to satisfy the voltages' constraints.

B. A Second Local Voltage Control Strategy (Denoted as LVC-2)

LVC-2 aims at driving all the compensators' voltage magnitudes to a desired value U_d. Again it is based only on local measurements, but differently from LVC-1, it does not resort to a droop-like function as the one introduced in (V-A). Specifically, agent h updates the amount of reactive power to be injected as

$$q_h(t+1) = [q_h(t) + \epsilon\,(U_d - v_h(t))]_{q_{\min}}^{q_{\max}} \tag{16}$$

where ϵ is a positive constant. Loosely speaking, the rationale behind LVC-2 is as follows: if $v_h < U_d$ then agent h will inject reactive power in order to increase v_h, while if $v_h > U_d$ then agent h will absorb reactive power in order to decrease v_h. The convergence properties of LVC-2 are next stated.

Proposition 2: Consider algorithm (16). Then, if

$$\epsilon \leq \frac{2U_N}{\rho(\Im(M))} \tag{17}$$

there exist a m-upla $(\bar{v}_1, \ldots, \bar{v}_m)$ such that $v_h(t) \to \bar{v}_h$ for all $h \in \{1, \ldots, m\}$.

Observe that the Proposition 2, whose proof is reported in the Appendix, establishes that, if ϵ satisfies (17), then the voltages magnitudes converge to steady state values $(\bar{v}_1, \ldots, \bar{v}_m)$. However, in general, it is not guaranteed that $\bar{u}_h = U_d$ for all $h \in \{1, \ldots, m\}$, and that $\bar{v}_h \in [U_{\min}, U_{\max}]$, even if $U_d \in [U_{\min}, U_{\max}]$. In Section VII we will provide a numerical example where, though $U_d \in [U_{\min}, U_{\max}]$, there exists at least one agent h such that $\bar{v}_h \notin [U_{\min}, U_{\max}]$.

Remark 4: The LVC-2 is very similar to the classic integral secondary voltage control used in transmission network to provide generator reactive power control, but confined to a single generator. Both of them update the reactive power output based on a feedback of the actual voltage magnitude. Furthermore, it is very similar to the method illustrated in [14], where the more general update step $q_h(t+1) = [(1 - \epsilon c_h)\, q_h(t) + \epsilon(U_d - v_h(t))]_{q_{\min}}^{q_{\max}}$ has been proposed (being c_h a suitable positive parameter). However, we stress that LVC-2 strategy has been first presented in the conference paper [21] and we will see in Section VI that LVC-2 scheme will play an important role in designing a fast distributed optimal reactive power flow algorithm.

VI. A Fast Distributed Optimal Reactive Power Flow Algorithm (Denoted as f-DORPF)

In this section, we propose a novel *distributed* control algorithm where each agent h, beside local voltage measurements, requires additional information coming from the neighboring nodes in $\mathcal{N}(h)$ to update the reactive power output. In addition to a voltage regulation objective, the strategy exploits the cooperation among the agents to minimize the power losses on the electric lines; specifically, it aims at solving the following *optimal reactive power flow* (OPRF) problem

$$\min_{q_G} \quad \Re(\bar{u}^T Y u) \tag{18a}$$

$$\text{subject to } q_G \in \mathcal{F} \tag{18b}$$

where $\Re(\bar{u}^T Y u)$ are the line active power losses. Indeed, in [18] it is shown how, by exploiting (7), the line power losses can be expressed by (18a).

The algorithm is derived in the simplified scenario where all the grid power lines are assumed to have the same resistance/inductance ratio, i.e., there exists θ, such that

$$z_e = e^{i\theta}|z_e|. \tag{19}$$

for all $e \in \mathcal{E}$. Equation (19) is satisfied when the grid is relatively homogeneous, and is reasonable in most practical cases. However, in Section VII, we simulate the algorithm in the more realistic scenario where (19) does not hold. It can be shown (see [18] for the details) that, under approximation (7) and under (19), the cost function (18a) is a quadratic function on q_G and $\mathcal{F}$ is a convex set on q_G. Indeed, we have that

$$\Re(\bar{u}^T Y u) \simeq q_G^T \frac{\Re(M)}{U_N^2} q_G + 2 q_G^T \frac{\Re(N)}{U_N^2} q_L + q_L^T \frac{\Re(Q)}{U_N^2} q_L,$$

and that $\mathcal{F}$ can be conveniently approximated by

$$\tilde{\mathcal{F}} = \left\{ q_G : V_{\min} \leq \frac{\Im(M)}{U_N} q_G \leq V_{\max}, q_{\min} \leq q_G \leq q_{\max} \right\}$$

where

$$V_{\min} = -\frac{1}{U_N}\left(\Re \begin{bmatrix} M & N \end{bmatrix} \begin{bmatrix} p_G \\ p_L \end{bmatrix} - \Im(N) q_L \right) + \mathbf{1}(U_{\min} - U_N),$$

$$V_{\max} = -\frac{1}{U_N}\left(\Re \begin{bmatrix} M & N \end{bmatrix} \begin{bmatrix} p_G \\ p_L \end{bmatrix} - \Im(N) q_L \right) + \mathbf{1}(U_{\max} - U_N).$$

Therefore, problem (18) can be convexified obtaining

$$\min_{q_G} \quad q_G^T \frac{\Re(M)}{U_N^2} q_G + 2 q_G^T \frac{\Re(N)}{U_N^2} q_L + q_L^T \frac{\Re(Q)}{U_N^2} q_L \tag{20a}$$

$$\text{subject to } q_G \in \tilde{\mathcal{F}}. \tag{20b}$$

We refer to the above problem as the *approximated convexified (OPRF) problem* and we denote by q_G^* its optimal solution.

The f-DORPF algorithm improves the performance of the algorithm presented in [18] (denoted hereafter as DORPF). DORPF addresses problem (18) by a iterative dual ascent strategy adopting auxiliary variables, i.e., the *Lagrange multipliers*, for both the voltage and the reactive power constraints. Differently from LVC-1 and LVC-2, agents in DORPF can communicate with their neighbors. Remarkably, it is shown in [18] that,

under (7), (19) and some additional mild assumptions, DORPF converges to q_G^*, the optimizer of the approximated convexified OPRF problem. In other words, thanks to the additional information received from the neighbors, the agents not only drive the voltage magnitudes to satisfy the operational constraints, but also minimize the power losses. However, in spite of this optimal steady-state property, experimental results show how the transient of DORPF is much slower than the one of the local algorithms.

In this section, to improve the transient performance of DORPF, we introduce the f-DORPF algorithm, obtained by combining DORPF with LVC-2. Numerical results reported in Section VII show how f-DORPF inherits the fast transient of LVC-2 and the convergence to the optimal equilibrium of DORPF. The f-DORPF algorithm is still an iterative dual-ascent like strategy where only the Lagrange multipliers associated to the reactive power constraints are introduced. Eliminating the Lagrange multipliers related to voltages' constraints speeds up significantly the transient of the DORPF algorithm; in f-DORPF, the absence of the voltages' multipliers is compensated by the fact that agent h performs a step of LVC-2 whenever $v_h < U_{\min}$ or $v_h > U_{\max}$. An algorithmic description of f-DORPF is provided in Algorithm 1 where, for each agent h, $\mu_{\text{min,h}}$ and $\mu_{\text{max,h}}$ denote the Lagrange multipliers associated with the constraints $q_h \geq q_{\min}$ and $q_h \leq q_{\max}$, respectively. Moreover, the symbol $y_{h\ell}$ denotes the admittance of the electrical path between agents h and ℓ which is assumed to be known by both agent h and agent ℓ. Also the positive parameters ϵ and γ are assumed to be a-priori assigned (in particular, ϵ satisfying (17)).

Some explanations are in order. If v_h violates constraint (9), agent h updates its reactive power by using the LVC-2 rule, once set $U_d = U_N$ (see (21)).

Instead, if $v_h \in [U_{\min}, U_{\max}]$, then agent h discriminates between a step inspired by DORPF (see (22) and the algorithm presented in Section VI in [18]), and a step of LVC-2 (see (23) and (24) obtained by setting, respectively, $U_d = U_{\max}$ and $U_d = U_{\min}$). Observe that the term $\delta_{f,h}$ involves the knowledge of multipliers of h and of its neighbors; therefore its computation requires the communication between neighboring agents. Notice that the terms $\delta_{U_{\max},h}$ and $\delta_{U_{\min},h}$ have, by definition, different signs. Let $\tilde{\delta}$ be the one with the same sign of $\delta_{f,h}$. The h's reactive power increments $\delta_{f,h}$ and $\tilde{\delta}$ have the same effect on h's voltage magnitude: either an increment (if both positive) or a decrement (if both negative). Finally, f-DORPF chooses the less aggressive update between $\delta_{f,h}$ and $\tilde{\delta}$ (see (25)).

A note is required about $\delta_{f,h}$. As written above, (22) has been inspired by the update proposed in DORPF, where, however, an additional term was included in computing the updated amount of reactive power to be injected; this term was related to the Lagrange multipliers associated with the voltage constraints.[1] Since voltage Lagrange multipliers are missing in f-DORPF, we expect that the mere use of (22) might drive the voltage magnitudes outside the range $[U_{\min}, U_{\max}]$, though moving the system towards the minimum losses configuration. This observation is also consistent with the results illustrated in [22], where an update rule of q_h based only on $\delta_{f,h}$ has been proposed and fully analyzed; indeed, the goal in [22] was only that of minimizing the power losses under solely generation limits and ignoring the presence of voltage constraints. Based on the above observations, in f-DORPF we do not rely only on (22), but the actual amount of reactive power to be injected by agent h is obtained by comparing $\delta_{f,h}$ with $\delta_{U_{\max},h}$ and $\delta_{U_{\min},h}$.

[1]Specifically in DORPF we have $\delta = \sum_{\ell\in\mathcal{N}(h)}(\mu_{\min,\ell}(t) - \mu_{\max,\ell}(t) + y_{h\ell}v_h(t)v_k(t)\sin(\angle u_\ell(t) - \angle u_h(t) - \theta)) - \sin\theta(\lambda_{\text{max,h}}(t) - \lambda_{\text{min,h}}(t))$ where $\lambda_{\text{max,h}}$ and $\lambda_{\text{min,h}}$ are the Lagrange multipliers associated to $q_h \leq q_{\max}$ and $q_h \geq q_{\min}$, respectively.

Algorithm 1: f-DORPF.

Require: At each time t, agent h

gathers $\mu_k(t-1), k \in \mathcal{N}(h)$, and measures $u_h(t), v_h(t)$.

if $v_h(t) \geq U_{\max}$ or $v_h(t) \leq U_{\min}$ **then**

$$\delta_h = \epsilon(U_N - v_h(t)) \tag{21}$$

end if

if $U_{\min} < v_h(t) < U_{\max}$ **then**

computes

$$\delta_{f,h} = \sum_{\ell\in\mathcal{N}(h)} \Big(\mu_{\text{min},\ell}(t) - \mu_{\text{max},\ell}(t) + y_{h\ell}v_h(t)v_k(t)\sin(\angle u_\ell(t) - \angle u_h(t) - \theta)\Big) \tag{22}$$

$$\delta_{U_{\max},h} = \epsilon(U_{\max} - v_h(t)) \tag{23}$$

$$\delta_{U_{\min},h} = \epsilon(U_{\min} - v_h(t)) \tag{24}$$

and sets

if $\text{sign}(\delta_{U_{\min},h}) = \text{sign}(\delta_{f,h})$**then**

$\tilde{\delta} = \delta_{U_{\min},h}$

else

$\tilde{\delta} = \delta_{U_{\max},h}$

end if

$$\delta_h = \text{sign}(\delta_{f,h})\min\{\delta_{f,h}, \tilde{\delta}\} \tag{25}$$

end if

computes the reactive power update

$$\tilde{q}_h = q_h(t) + \delta_h \tag{26}$$

computes the Lagrange multipliers update

$$\mu_{\min,h}(t+1) = \left[\mu_{\text{min},h}(t) + \gamma\left(\frac{q_{\min}}{U_N^2} - \frac{\tilde{q}_h}{U_N^2}\right)\right]_0^\infty \tag{27}$$

$$\mu_{\max,h}(t+1) = \left[\mu_{\max,h}(t) + \gamma\left(\frac{\tilde{q}_h}{U_N^2} - \frac{q_{\max}}{U_N^2}\right)\right]_0^\infty \tag{28}$$

injects the projected setpoints

$$q_h(t+1) = [\tilde{q}_h]_{q_{\min}}^{q_{\max}} \tag{29}$$

Regarding the step-size parameters ϵ and γ, we assume that ϵ satisfies (17) (as in LVC-2) and that γ is such that

$$\gamma \leq 2U_N \,/\, \rho(M^{-1}) \tag{30}$$

The latter condition is inherited from the similarity discussed above between the update in (22) and the algorithm in [22] where the derivation of (30) can be found.

The f-DORPF guarantees that the voltage constraints are satisfied asymptotically. This might be acceptable, in the meaning that voltage constraints can be intended as soft constraints, since they do not derive from physical constraints on the system, and their violation can be tolerated if it affects the system for a small time lapse. On the other hand, the power generation constraints are met at each iteration, since they stems from physical limitations of the generators, and they have to be intended as hard constraints.

We conclude this subsection by highlighting another interesting property of the f-DORPF. Agent h updates the Lagrange multipliers $\mu_{\min,h}$, $\mu_{\max,h}$ (by (27) and (28)) at each iteration of the algorithm, also when the value of δ_h does not depend on $\mu_{\min,h}$ or $\mu_{\max,h}$, i.e., when the amount of reactive power to be injected is computed according to a LVC-2 step. Nonetheless, the updated values of $\mu_{\min,h}$ and $\mu_{\max,h}$ are broadcasted to agents in $\mathcal{N}(h)$, that use them to perform computations in (22); likely, some of the reactive power set points computed by agents in $\mathcal{N}(h)$ will depend on these values of $\mu_{\min,h}$ and $\mu_{\max,h}$. This information flow is crucial to meet the operative constraints; indeed it is thanks to this cooperation that agents are able to rise o decrease the voltage magnitude of those agents, which are operating at their limits (in terms of reactive power injection), but are violating the voltage constraints.

A. On the Equilibrium Points of the f-DORPF

In the following Proposition we characterize the equilibrium points of the f-DORPF algorithm by assuming that the grid is radial, which is always the case of distribution networks.

Proposition 3: Consider the f-DORPF algorithm and assume the grid radial. Let q_G^* be the optimal solution of the approximated convexified OPRF problem. Then the following two facts hold true:

1) There exist $(\mu^*_{\max}, \mu^*_{\min})$ such that $(q_G^*, \mu^*_{\max}, \mu^*_{\min})$ is an equilibrium for the f-DORPF; and
2) If $(\tilde{q}_G, \tilde{\mu}_{\max}, \tilde{\mu}_{\min})$ is an equilibrium for the f-DORPF, then $\tilde{q}_G = q_G^*$.

The proof of the proposition is reported in the Appendix. Observe that Proposition 3 does not guarantee the existence of a unique equilibrium point for f-DORPF. What is shown is that, if $(\bar{q}_G, \bar{\mu}_{\max}, \bar{\mu}_{\min})$ is an equilibrium then $q_G = q_G^*$ where q_G^* is the optimal solution to the approximated convexified ORPF problem In other words, the uniqueness is guaranteed in terms of reactive power injected into the grid, that, at any equilibrium, is equal to q_G^*. Moreover Proposition 3 states also, that if the feasible set $\mathcal{F}$ is not empty, then there exists also an equilibrium point for f-DORPF.

Remark 5: We remark how f-DORPF algorithm can be considered as a *feedback control* strategy. Indeed, a key feature of f-DORPF is that it requires the alternation of measurement and actuation based on the measured data, and therefore it is inherently an online algorithm. Moreover not all the buses need to be monitored as required in the standard approaches adopted to solve ORPF problem; the reactive power injection of the generators is adjusted by f-DORPF based on the phasorial voltage measurements that are performed only at the buses where the generators are connected. Observe that agents actuate the system at every iteration, by updating the amount of reactive power that the agents command to the generators. Only by doing so, the subsequent measurement of the voltages will be informative of the new state of the system. The resulting control strategy is thus a feedback strategy that necessarily requires the real- time interaction of the controller (the cyber layer) with the plant (the physical layer). This tight interaction between the cyber layer and the physical layer is the fundamental feature of the proposed approach, and allows to drive the system towards the optimal configuration, which depends also on the reactive power demand of the loads, without collecting this information from them. In a sense, the algorithm is inferring this hidden information from the measurement performed on the system during its execution.

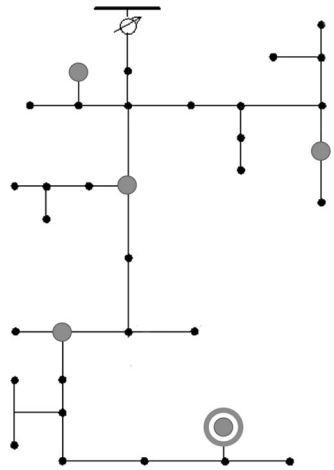

Fig. 4. Schematic representation of the IEEE 37 test feeder [23], the agents are represented by gray nodes in the distribution network.

VII. Simulations and Discussion

The algorithms have been simulated on testbeds inspired from the IEEE 37 and the IEEE 123 (see [23]), depicted in Figs. 4 and 5. In this case both the assumptions on homogeneous micro-generators and homogeneous line impedances do not hold; thus, the algorithms are tested in a realistic scenario. We consider the scenario where several micro-generators, gray nodes in Figs. 4 and 5, can regulate the reactive power injection to control the voltage magnitude.

The algorithms presented have been run on a nonlinear exact solver of the grid [24]. In all the simulations, the reactive power outputs of the micro-generators have been initialized to zero, while their generation capabilities have been chosen such that $\mathcal{F}$ is nonempty for any t, namely there is always a feasible solution. The minimum and the maximum tolerated voltage magnitude are $U_{\min} = 0.95$ and $U_{\max} = 1.05$, respectively. The

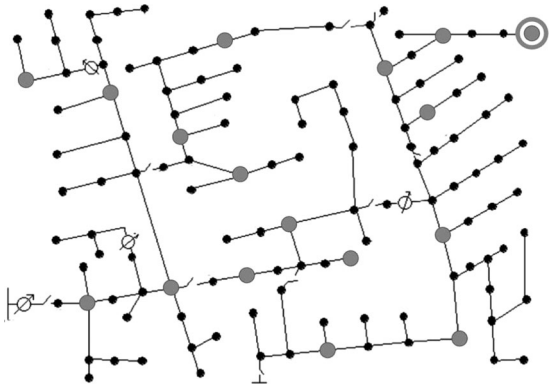

Fig. 5. Schematic representation of the IEEE 123 test feeder [23], the agents are represented by gray nodes in the distribution network.

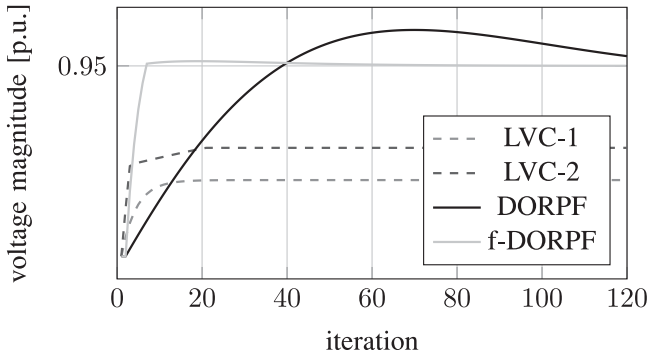

Fig. 6. Minimum compensators voltage magnitude (attained at the circled grey node in Fig. 4) in the IEEE37 test case.

simulations have been obtained setting the parameters α, ϵ and γ at the limit values defined, respectively, in (14), (17) and (30), namely, in the IEEE37 testbed

$$\alpha = 0.16, \epsilon = 3.09, \gamma = 5.30 \cdot 10^{-2}$$

while in the IEEE123 testbed

$$\alpha = 0.14, \epsilon = 4.96, \gamma = 8.61 \cdot 10^{-4}.$$

A. Static Load Analysis

In this subsection we compare the algorithms performance when the grid loads are time-invariant. In Figs. 6 and 7 we plot the voltage magnitude profile of the agent achieving the smallest value at the steady state, i.e., the agent circled in Figs. 4 and 5.[2] Notice that, though the system is feasible, LVC-1 and LVC-2 fail to meet the voltage constraints in the IEEE37 case (see Fig. 6). This is a consequence of the lack of cooperation among the microgenerators, as discussed more in depth in [25]. Nonetheless, the general effect of LVC-1 and LVC-2 is that of moving the voltage magnitude towards the feasible set; indeed, the distance of the steady-state voltage magnitude from $U_{\min}$ is smaller than the distance of the initial voltage magnitude from $U_{\min}$. In Fig. 7 all the strategies lead the voltage magnitude within $[U_{\min}, U_{\max}]$; in this case, we highlight the fast transient of LVC-1, LVC-2

[2]For simplicity we consider only the constraint $v_h \geq U_{\min}$.

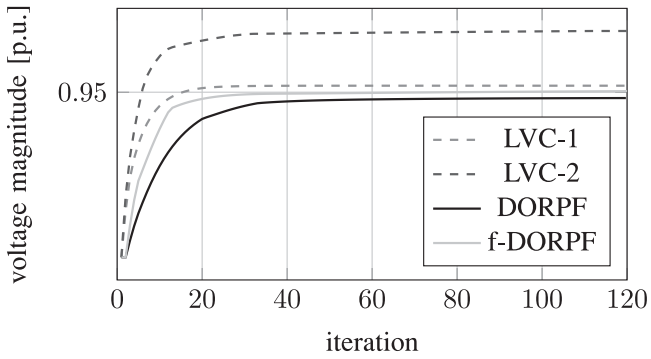

Fig. 7. Minimum compensators voltage magnitude (attained at the circled grey node in Fig. 5) in the IEEE123 test case.

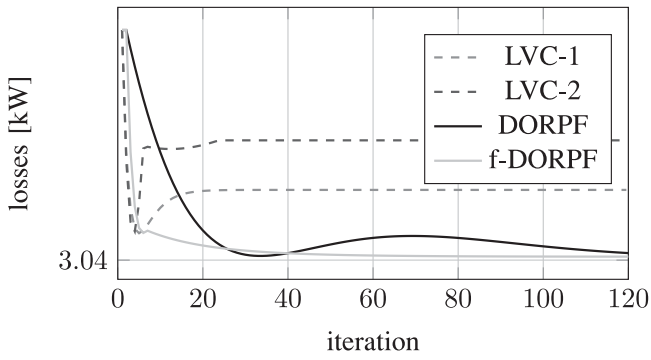

Fig. 8. System losses using the DORPF and the f-DORPF. The losses minimum value of this particular realization, computed via a centralized solver, is of 3.04 kW.

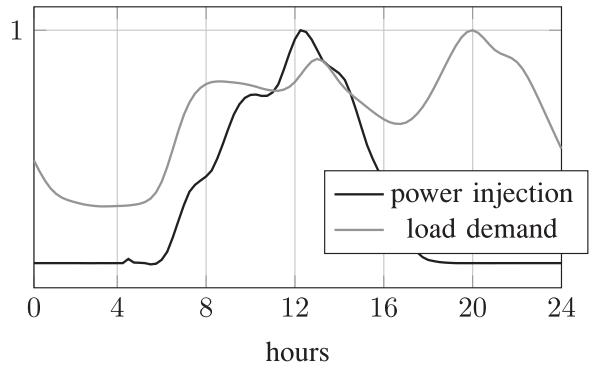

Fig. 9. Daily behaviour of power generation and of load demand.

and how f-DORPF significantly improves the performance of DORPF.In Fig. 8 we report the behavior of the power losses in the IEEE37 test case. Observe that f-DORPF attains the same steady-state value of the DORPF, exhibiting a faster transient. Instead, LVC-1 and LVC-2, not aiming at minimizing the losses, lead the system to a less efficient configuration.

B. Dynamic Load Analysis

In this subsection we the compare algorithms performance when the loads are time varying. In Fig. 9 the daily profiles, considered in the simulations, of both the total load demand and of the total active power injected by the agents into the grid, are

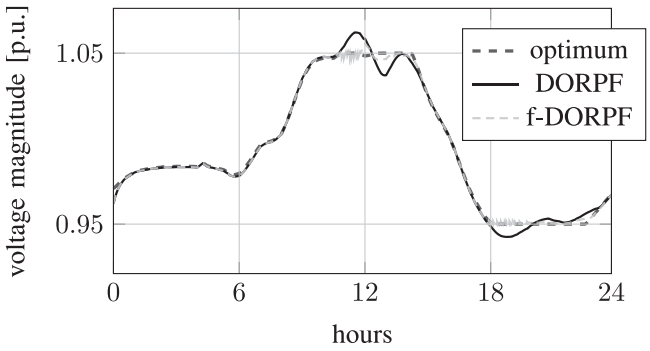

Fig. 10. Voltage magnitude profile of the circled agent in Fig. 4.

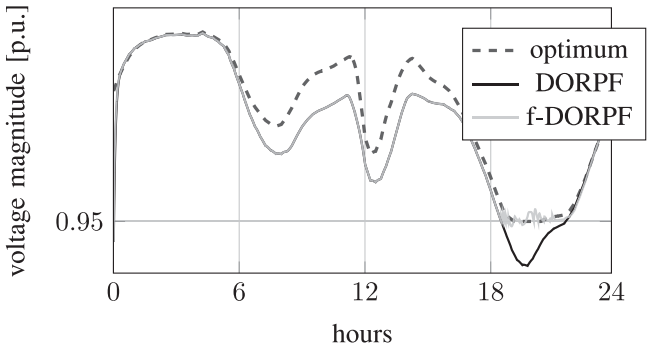

Fig. 11. Voltage magnitude profile of the circled agent in Fig. 5.

reported. Both profiles are normalized with the respect to the maximum value assumed during the day.

Typically, the inverter of agent h has an instantaneous generation capability which is limited by its fixed apparent power capability $|s_{\max,h}|$; namely, the phasor representing the instantaneous power injected must lie inside a circle of ray $|s_{\max,h}|$ centered at the origin. In our simulations, we assume $|s_{\max,h}| = 1.1 p_{\max,h}$, where $p_{\max,h}$ is the maximum amount of active power that can be generated, as suggested in [9], since inverters are available in discrete sizes and are likely to be slightly oversized with the respect to $p_{\max,h}$. It turns out that the amount of reactive power that can be injected by agent h at time t is a function of $|s_{\max,h}|$ and of the injected active power $p_h(t)$, i.e.,

$$q_{\max,h}(t) = \sqrt{|s_{\max,h}|^2 - p_h(t)^2}$$

and $q_{\min,h}(t) = -q_{\max,h}(t)$. The control actions are performed every 30 seconds. The results are reported in Figs. 10 and 11, where we plotted the daily behavior of the voltage magnitude of the circled agent in the IEEE37 and in the IEEE123 testbeds.

The following observations are in order. Firstly, when there are no voltage constraints violations, the trajectories described by DORPF and f-DORPF are basically the same; in other words f-DORPF acts as DORPF, thus attaining power losses minimization. Secondly, during the central hours of the day, in the IEEE37 testbed an overvoltage occurs due to the massive increment of active power injected. Notice that, it takes a while for DORPF to drive the voltage magnitude below the limit value $U_{\max}$; instead, f-DORPF is able to keep the constraints satisfied (i.e., the overvoltage is avoided) and generates a trajectory which is very close to the optimal one. Thirdly, during evening hours, the injection of active power significantly decreases causing an undervoltage. Again f-DORPF exhibits a superior performance with the respect to DORPF; no undervoltage appears in the trajectory depicted by f-DORPF, while it is not avoided when DORPF is adopted.

The better performance of f-DORPF in tracking the optimal solution in the more realistic scenario of time-varying loads, is related to its faster transient property we highlighted in the previous numerical example and in Section VI.

VIII. Conclusion

In this paper we propose and analyze, theoretically and through simulations, three voltage control strategies. The LVC-1 and the LVC-2 algorithms are purely local: the agents regulate their reactive power output based only on the knowledge of the magnitude of their own voltage. Since they do not require any communication infrastructure, they can be easily implemented but it is not guaranteed that the voltage constraints are met. Instead, the f-DORPF algorithms is distributed: the reactive power setpoints are computed by the agents exploiting both local measurements and information coming from the neighbors. This cooperation is exploited to not only satisfy the voltage requirements, but also to achieve the power losses optimality. The f-DORPF has been designed by combining DORPF (a distributed algorithm presented in [18] solving the optimization problem (20)) and LVC-2. Specifically, f-DORPF inherits the fast transient of LVC-2 and the steady state optimality property of DORPF. Simulations, illustrating the effectiveness of f-DORPF, are provided.

Appendix

Proof of Proposition 1: the component wise reactive power update (13) can be expressed in vectorial form as

$$q_G(t+1) = \left[\left(I + \frac{\alpha\zeta \Im(M)}{U_N} - \alpha I \right) q_G(t) + \alpha\zeta \tilde{V} + \alpha\beta \right]_{q_{\min}}^{q_{\max}},$$

where $\tilde{V} = \frac{\Im(N)}{U_N} q_L + \frac{\Re[\,M\ N\,]}{U_N} [\,p_G\ p_L\,]^T + \mathbf{1}U_N$. Notice that $\tilde{V}$ represents the contribution of the uncontrolled powers p_G, p_L, q_L to the agents voltage magnitude, i.e., $v_G = \frac{\Im(M)}{U_N} q_G + \tilde{V}$. Let us define $x(t) = q_G(t) - q_G(k-1)$. By exploiting the fact that given the vectors v, w, a, b, $\|[v]_a^b - [w]_a^b\| \leq \|v - w\|$, it can be easily shown that

$$\|x(t+1)\| \leq \|(I + \alpha\zeta\Im(M)/U_N - \alpha I)\| \, \|x(t)\|. \quad (31)$$

From (31) it follows that if (14) holds, then $\|x(t)\| \to 0$, $q_G(t) \to \bar{q}_G$, and $\bar{q}_G$ is associated with $(\bar{u}_1, \ldots, \bar{u}_m)$. ■

Proof of Proposition 2: The component wise reactive power update (16) can be expressed in vectorial form as

$$q_G(t+1) = \left[(I - \epsilon\Im(M)/U_N)\, q_G(t) + \epsilon \left(u_d - \tilde{V} \right) \right]_{q_{\min}}^{q_{\max}}, \quad (32)$$

where $\tilde{V}$ is defined as previously, as the variable $x(t)$. Then

$$\|x(t+1)\| \leq \|I - \epsilon \Im(M)/U_N\| \, \|x(t)\| \tag{33}$$

It is thus straightforward to see that if condition (17) holds, $\|x(t)\| \to 0$ then $q_G(t) \to \bar{q}_G$, with $\bar{q}_G$ associated with the voltages $(\bar{u}_1, \ldots, \bar{u}_m)$. ■

Proof of Proposition 3: Consider problem (20). Since it is convex, standard optimization results (see [26]) show that, for suitable values of γ, the dual ascent strategy (see [18])

$$\begin{aligned}
q_G(t+1) &= q_G(t) + \delta_D(q_G(t), \lambda_{\min}(t), \lambda_{\max}(t), \\
&\qquad \mu_{\max}(t), \mu_{\min}(t)) \\
\lambda_{\min,h}(t+1) &= \left[\lambda_{\min,h}(t) + \frac{\gamma}{U_N^2}\left(U_{\min}^2 - v_h(t)^2\right)\right]_0^\infty \\
\lambda_{\max,h}(t+1) &= \left[\lambda_{\max,h}(t) + \frac{\gamma}{U_N^2}\left(v_h(t)^2 - U_{\max}^2\right)\right]_0^\infty \\
\mu_{\min,h}(t+1) &= \left[\mu_{\min,h}(t) + \frac{\gamma}{2U_N^2}\left(q_{\min} - \bar{q}_h\right)\right]_0^\infty \\
\mu_{\max,h}(t+1) &= \left[\mu_{\max,h}(t) + \frac{\gamma}{2U_N^2}\left(\bar{q}_h - q_{\max}\right)\right]_0^\infty,
\end{aligned}$$

where

$$\begin{aligned}
\delta_D(q_G, \lambda_{\min}, \lambda_{\max}, \mu_{\max}, \mu_{\min}) &= -q_G - M^{-1} N q_L \\
&\quad + \sin\theta(\lambda_{\min} - \lambda_{\max}) + M^{-1}(\mu_{\min} - \mu_{\max})
\end{aligned} \tag{34}$$

converges to $(q_G^*, \lambda_{\min}^*, \lambda_{\max}^*, \mu_{\min}^*, \mu_{\max}^*)$, being q_G^* the optimizer of problem (20). Let δ_f be the vector collecting all the $(\delta_f)_h$'s (defined in (22)), $h \in \mathcal{C}$. The vector δ_f can be expressed (see [18]) exploiting the linear model (8), as

$$\delta_f(q_G, \mu_{\max}, \mu_{\min}) = M^{-1}(\mu_{\min} - \mu_{\max}) - q_G - M^{-1} N q_L. \tag{35}$$

Let the equilibrium of the dual ascent strategy be $(q_G^*, \lambda_{\min}^*, \lambda_{\max}^*, \mu_{\min}^*, \mu_{\max}^*)$. It satisfies the condition

$$\delta_D(q_G^*, \lambda_{\min}^*, \lambda_{\max}^*, \mu_{\min}^*, \mu_{\max}^*) = 0.$$

We will show that $(q_G^*, \mu_{\min}^*, \mu_{\max}^*)$ is an equilibrium for the f-DORPF. Let h denote an agent whose multipliers $\lambda_{\min,h}^*, \lambda_{\max,h}^*$ are equal to zero. In this case, by comparing (34) and (35), it follows that

$$\delta_f(q_G^*, \mu_{\min}^*, \mu_{\max}^*) = \delta_D(q_G^*, \lambda_{\min}^*, \lambda_{\max}^*, \mu_{\min}^*, \mu_{\max}^*) = 0.$$

As a consequence, we have, from (25), that $\delta_h = 0$ for all $h \in \mathcal{C}$. Now, let h denote an agent such that either $\lambda_{\min,h}^*$ or $\lambda_{\max,h}^*$ is greater than zero. This implies that v_h is equal to either $U_{\min}$ or $U_{\max}$. Consider the case where $\lambda_{\min,h}^* > 0$ and $v_h = U_{\min}$ (the case where $\lambda_{\max,h}^* > 0$ and $v_h = U_{\max}$ is analogous). Being $v_h = U_{\min}$, from (23) and (24) it turns out that $\delta_{U_{\max,h}} > 0$ and $\delta_{U_{\min,h}} = 0$. Furthermore,

$$\delta_{f,h}(q^*, \mu_{\min}^*, \mu_{\max}^*) \leq \delta_{D,h}(q^*, \mu_{\min}^*, \mu_{\max}^*, \lambda_{\min}^*, \lambda_{\max}^*) = 0.$$

From (25), it follows that $\delta_h = 0$. Thus $(q_G^*, \mu_{\min}^*, \mu_{\max}^*)$ is an equilibrium for the f-DORPF. On the converse, let $(\tilde{q}_G, \tilde{\mu}_{\min}, \tilde{\mu}_{\max})$ be an equilibrium of the f-DORPF algorithm. Firstly, notice that $\tilde{q}_G$ belongs to $\tilde{\mathcal{F}}$. In fact, if $\tilde{q}_G \notin \tilde{\mathcal{F}}$, then there would be at least an agent h such that either $v_h < U_{\min}$ and $q_h = q_{\max}$, or $v_h > U_{\max}$ and $q_h = q_{\min}$. Consider the former case (the latter is analogous). From (27) and (28), it follows that $\tilde{\mu}_{\max,h}$ keeps increasing, and thus $(\tilde{q}_G, \tilde{\mu}_{\min}, \tilde{\mu}_{\max})$ is not an equilibrium. Hence $\tilde{q}_G \in \tilde{\mathcal{F}}$. Now, let us introduce the auxiliary variables $\tilde{\lambda}_{\min,h}$ and $\tilde{\lambda}_{\max,h}$, by

$$\tilde{\lambda}_{\min,h}\left(\tilde{\lambda}_{\max,h}\right) = \begin{cases} 0 & \left(\frac{\delta_{f,h}}{\sin\theta}\right) \quad \text{if } \delta_{f,h} \geq 0 \\ -\dfrac{\delta_{f,h}}{\sin\theta} & (0) \quad \text{if } \delta_{f,h} < 0. \end{cases}$$

Observe that both $\tilde{\lambda}_{\min}$ and $\tilde{\lambda}_{\max}$ have only non-negative entries and that $\delta_D(\tilde{q}_G, \tilde{\lambda}_{\min}, \tilde{\lambda}_{\max}, \tilde{\mu}_{\min}, \tilde{\mu}_{\max}) = 0$. Thus, since the minimizer is unique, $\tilde{q}_G = q_G^*$. ■

REFERENCES

[1] A. Ipakchi and F. Albuyeh, "Grid of the future," *IEEE Power Energy Mag.*, vol. 7, no. 2, pp. 52–62, Mar./Apr. 2009.

[2] F. Katiraei and M. Iravani, "Power management strategies for a microgrid with multiple distributed generation units," *IEEE Trans. Power Syst.*, vol. 21, no. 4, pp. 1821–1831, Nov. 2006.

[3] S. Corsi, *Voltage Control and Protection in Electrical Power Systems: From System Components to Wide-Area Control*. New York, NY, USA: Springer, 2015.

[4] S. Corsi, M. Pozzi, C. Sabelli, and A. Serrani, "The coordinated automatic voltage control of the Italian transmission grid—Part I: Reasons of the choice and overview of the consolidated hierarchical system," *IEEE Trans. Power Syst.*, vol. 19, no. 4, pp. 1723–1732, Nov. 2004.

[5] F. Dorfler, J. W. Simpson-Porco , and F. Bullo, "Breaking the hierarchy: Distributed control and economic optimality in microgrids," *IEEE Trans. Control Netw. Syst.*, vol. 3, no. 3, pp. 241–253, Sep. 2016.

[6] M. E. Baran and F. F. Wu, "Optimal sizing of capacitors placed on a radial distribution system," *IEEE Trans. Power Del.*, vol. 4, no. 1, pp. 735–743, Jan. 1989.

[7] K. Turitsyn, P. Šulc, S. Backhaus, and M. Chertkov, "Options for control of reactive power by distributed photovoltaic generators," *Proc. IEEE*, vol. 99, no. 6, pp. 1063–1073, Jun. 2011.

[8] M. Juamperez, Y. Guangya, and S. B. Kjær, "Voltage regulation in LV grids by coordinated volt-var control strategies," *J. Modern Power Syst. Clean Energy*, vol. 2, no. 4, pp. 319–328, 2014.

[9] S. Kundu, S. Backhaus, and I. A. Hiskens, "Distributed control of reactive power from photovoltaic inverters," in *Proc. IEEE Int. Symp. Circuits Syst.*, 2013, pp. 249–252.

[10] N. Li, G. Qu, and M. Dahleh, "Real-time decentralized voltage control in distribution networks," in *Proc. IEEE 52nd Annu. Allerton Conf. Commun. Control Comput.*, 2014, pp. 582–588.

[11] V. Kekatos, L. Zhang, G. B. Giannakis, and R. Baldick, "Voltage regulation algorithms for multiphase power distribution grids," *IEEE Trans. Power Syst.*, vol. 31, no. 5, pp. 3913–3923, Sep. 2016.

[12] M. Farivar, X. Zhou, and L. Chen, "Local voltage control in distribution systems: An incremental control algorithm," in *Proc. IEEE Int. Conf. Smart Grid Commun.*, 2015, pp. 732–737.

[13] M. Farivar, L. Chen, and S. Low, "Equilibrium and dynamics of local voltage control in distribution systems," in *Proc. IEEE 52nd Conf. Decis. Control*, 2013, pp. 4329–4334.

[14] H. Zhu and H. J. Liu, "Fast local voltage control under limited reactive power: Optimality and stability analysis," *IEEE Trans. Power Syst.*, vol. 31, no. 5, pp. 3794–3803, Sep. 2016.

[15] E. Dell'Anese, H. Zhu, and G. Giannakis, "Distributed optimal power flow for smart microgrids," *IEEE Trans. Smart Grid*, vol. 4, no. 3, pp. 1464–1475, Sep. 2013.

[16] J. Lavaei and S. H. Low, "Zero duality gap in optimal power flow problem," *IEEE Trans. Power Syst.*, vol. 27, no. 1, pp. 92–107, Feb. 2012.

[17] B. Zhang, A. Lam, A. Dominguez-Garcia , and D. Tse, "An optimal and distributed method for voltage regulation in power distribution systems," *IEEE Trans. Power Syst.*, vol. 30, no. 4, pp. 1714–1726, Jul. 2015.

[18] S. Bolognani, R. Carli, G. Cavraro, and S. Zampieri, "Distributed reactive power feedback control for voltage regulation and loss minimization," *IEEE Trans. Autom. Control*, vol. 60, no. 4, pp. 966–981, Apr. 2015.

[19] F. Dorfler and F. Bullo, "Kron reduction of graphs with applications to electrical networks," *IEEE Trans. Circuits Syst. I, Reg. Papers*, vol. 60, no. 1, pp. 150–163, Jan. 2013.
[20] *IEEE Draft Recommended Practice for Establishing Methods and Procedures That Provide Supplemental Support for Implementation Strategies for Expanded Use of IEEE Standard 1547*, IEEE P1547.8/D8, Jul. 2014, pp. 1–176, Nov. 2014.
[21] R. Carli and G. Cavraro, "Algorithms for voltage control in distribution networks," in *Proc. IEEE Int. Conf. Smart Grid Commun.*, Nov. 2015, pp. 737–742.
[22] S. Bolognani, R. Carli, G. Cavraro, and S. Zampieri, "A distributed control strategy for optimal reactive power flow with power constraints," in *Proc. IEEE 52nd Annu. Conf. Decis. Control*, 2013, pp. 4644–4649.
[23] W. H. Kersting, "Radial distribution test feeders," in *Proc. IEEE Power Eng. Soc. Winter Meeting*, vol. 2, Jan. 2001, pp. 908–912.
[24] R. D. Zimmerman, C. E. Murillo-Sánchez, and R. J. Thomas, "MATPOWER: Steady-state operations, planning and analysis tools for power systems research and education," *IEEE Trans. Power Syst.*, vol. 26, no. 1, pp. 12–19, Feb. 2011.
[25] G. Cavraro, S. Bolognani, R. Carli, and S. Zampieri, "The value of communication in the voltage regulation problem," in *Proc. IEEE 55th Conf. Decis. Control*, Dec. 2016, pp. 5781–5786.
[26] D. P. Bertsekas and J. N. Tsitsiklis, *Parallel and Distributed Computation: Numerical Methods*. Belmont, MA, USA: Athena Scientific, 1997.

Guido Cavraro received the B.S. degree in information engineering, the M.S. degree in automation engineering, and the Ph.D. degree in information engineering from the University of Padova, Padova, Italy, in 2008, 2011, and 2015, respectively. In 2015 and 2016, he was a Postdoctoral Associate in the Department of Information Engineering, University of Padova. He is currently a Postdoctoral Associate in the Bradley Department of Electronics and Communication Engineering, Virginia Tech, Blacksburg, VA, USA. His current research interests include identification, control and optimization applied to power systems and smart grids.

Ruggero Carli received the Laurea degree in computer engineering and the Ph.D. degree in information engineering from the University of Padova, Padova, Italy, in 2004 and 2007, respectively. From 2008 to 2010, he was a Postdoctoral Fellow with the Department of Mechanical Engineering, University of California at Santa Barbara, Santa Barbara, CA, USA. He is currently an Associate Professor with the Department of Information Engineering, University of Padova. His research interests include control theory and, in particular, control under communication constraints, cooperative control, and distributed estimation.